Available online at www.sciencedirect.com
ScienceDirect
Journal of Chromatography A, 1131 (2006) 185–191
JOURNAL OF CHROMATOGRAPHY A
www.elsevier.com/locate/chroma

Effect of dissolution temperature on the structures of sodium hyaluronate by flow field-flow fractionation/multiangle light scattering

Heejeong Lee [a], Il-Hwan Cho [b], Myeong Hee Moon [a,*]

[a] *Department of Chemistry, Yonsei University, Seoul, 120-749, South Korea*
[b] *Department of Biotechnology, Shinpoong Pharmaceutical, Co. Ltd., Ansan, Kyeonggi-Do, South Korea*

Received 1 March 2006; received in revised form 15 July 2006; accepted 21 July 2006
Available online 8 August 2006

Abstract

Molecular weight distribution (MWD) and structural deformation of ultrahigh molecular weight (MW) sodium hylaluronate (10^5–10^8 g/mol) were studied under different sample dissolution temperature conditions, using on-line flow field-flow fractionation (FlFFF) and multiangle light scattering (MALS). Sodium hyaluronate (NaHA) materials from sarcoma fluid have been studied by dissolving them in water at three different temperature conditions (5 °C, 50 °C, and 90 °C). Frit inlet asymmetrical flow field-flow fractionation (FI-AFlFFF), with field programming, was utilized for the separation of NaHA by MW, and on-line observation of light scattering of fractionated NaHA by MALS was performed in order to determine the MWD and molecular conformation. In these experiments, NaHA molecules exhibited an extended structure from a formerly rather compact geometry when the dissolving temperature was raised to 90 °C. This study also showed a clear difference in the MWD of NaHA when a preliminary filtration process was applied.

Keywords: Sodium hyaluronate; Sarcoma fluid; Field-flow fractionation; Field programming; Multiangle light scattering; Molecular weight distribution; NaHA structure

1. Introduction

Sodium hyaluronate (NaHA), a sodium salt of hyaluronic acid (HA), is a polysaccharide with a regularly alternating disaccharide unit (D-glucronic acid and *N*-acetyl-D-glucosamine) that can be found in various body fluids or tissues in nature [1–3]. NaHA is a major component of the vitreous humor, where it behaves as an optically transparent, low-refractive-index gel in the eyeball, and also of synovial fluid [4,5]. It is also used for various therapeutic, cosmetic, and pharmaceutical purposes [6–8]. The biological functions and applicability of NaHA are very much dependent on the molecular mass distribution, which may be as high as 10^7 g/mol [9]. Determination of the molecular weight of NaHA has been achieved by size exclusion chromatography (SEC), coupled with viscometric measurements [10] or matrix-assisted laser desorption ionization mass spectrometry (MALDI-MS) [1]. However, it is difficult to successfully fractionate polydispersed NaHA material with a molecular weight above a few million g/mol due to the exclusion limit of the gel matrix used in SEC. In addition, it may cause a shear induced degradation of NaHA molecules during penetration through gels or may encounter surface interaction with packing materials. Capillary electrophoresis was utilized as an alternative without using a packed column system [11], but this study relied on an external calibration method using pullulan standards of which chemical composition and structure were different from those of NaHA. High performance anion-exchange chromatography has also been utilized for the characterization of NaHA with NaHA standards [9] whose molecular weight values were measured by LALLS. However, this also is an indirect calculation of MW using a calibration method and contains a risk of sample interaction with the packed column system.

Flow field-flow fractionation (FlFFF) is an alternative method to separate high molecular weight polymers with the advantage of bypassing such potential problems explained above, since FlFFF is performed in a thin, empty channel. FlFFF has been utilized for the separation and characterization of particles and macromolecules, such as water-soluble polymers, proteins,

* Corresponding author. Tel.: +82 2 2123 5634; fax: +82 2 364 7050.
E-mail address: mhmoon@yonsei.ac.kr (M.H. Moon).

0021-9673/$ – see front matter © 2006 Elsevier B.V. All rights reserved.
doi:10.1016/j.chroma.2006.07.049

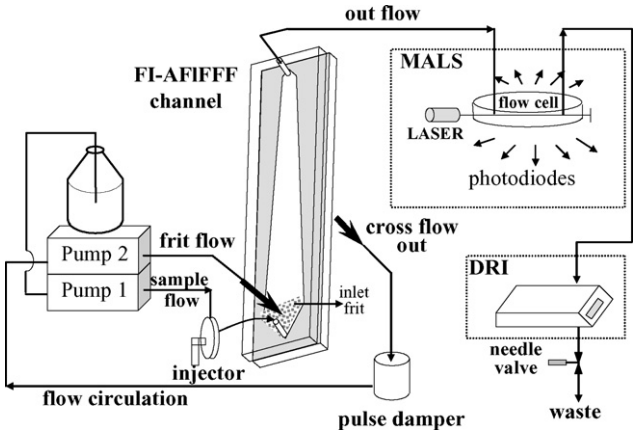

Fig. 1. Schematic diagram of the FI-AFlFFF channel with MALS/DRI detection.

DNA, and cells [12–16]. On-line coupling of FlFFF with multiangle light scattering (MALS) has gained increasing interest for the characterization of polymers [17–23]. When MALS is connected to the FlFFF channel, the combined method allows measurement of both molecular weight distribution (MWD) and the conformational information of the polymer sample by examining scattered light signals at different angles during the elution of fractionated molecules at each narrow volume slice. Recently, the on-line use of MALS with FlFFF has been applied to the separation of NaHA molecules [8,24]. Most studies on FlFFF/MALS have applied to the use of a conventional asymmetrical FlFFF (or AFlFFF) channel, which utilizes the focusing/relaxation process [23] requiring a stoppage of sample migration before separation begins. The previous study [24] demonstrated the successful use of the frit inlet asymmetrical flow field-flow fractionation (FI-AFlFFF) for continuous flow separation of ultrahigh MW NaHA materials by employing a field programming technique and for size characterization with the on-line connection to MALS. In the field programming, the cross flow rate is gradually decreased during the run to enhance the elution of long-retaining, high molecular weight polymers. FI-AFlFFF (shown in Fig. 1) is a variant of a flow field-flow fractionation technique that has been developed to perform sample relaxation without stopping the migration flow [25–28]. This feature can minimize the chance of sample adhesion at the accumulation wall since sample migration needs not be stopped for relaxation, as normally required in conventional FlFFF systems. Especially for polymeric materials that easily form aggregates, the hydrodynamic relaxation method can be helpful even though it does not provide a complete relaxation of injected sample components.

In this study, the influence of sample dissolution temperature on the MW and conformation of NaHA molecules is examined by FI-AFlFFF/MALS. MWDs of NaHA samples with different temperature preparations are compared to each other, and this study focused on the possibility of degradation, disagglomeration, and extension of complicated NaHA molecues according to the temperature conditions during sample dissolution. The advantage of employing the FlFFF technique for the characterization of ultrahigh MW polymers, without prior filtration of the sample solution, a step not required in F1FFF, is also demonstrated.

2. Experimental

2.1. Materials and reagents

Two NaHA samples were obtained from Shinpoong Pharm. Co. Ltd. (Ansan, Korea) which were extracted from fowl sarcoma fluid. Each sample was dissolved at a concentration of 1.0 mg/mL in FI-AFlFFF carrier solution: 0.1 M $NaNO_3$ solution containing 0.02% NaN_3 as bactericide. The carrier solution (total I = 0.103 M) was prepared from deionized water (>18 M Ω-cm) and filtered with a membrane filter (pore size = 0.1 μm) prior to use. Twenty microliters of each dissolved sample solution was injected for each FI-AFlFFF/MALS run. Each sample was dissolved by varying the temperature at 5 °C, 50 °C, and 90 °C without stirring in order to reduce any degradation of the NaHA molecules. Dissolution of NaHA at 5 °C was achieved by keeping the sample vial in the refrigerator for at least 24 h. When dissolving the samples at higher temperatures, a Reacti-Therm Heating/Stirring Module from Pierce (Rockford, IL, USA) was utilized without stirring.

2.2. FI-AFlFFF

The FI-AFlFFF channel was built in-house and was the same utilized in an earlier study [24]. A schematic of the current experimental setup is shown in Fig. 1. The channel dimensions are 27.2 cm of tip-to-tip length, with 2.0 cm of initial breadth and 1.0 cm of final breadth in a trapezoidal shape. The channel spacer is a Mylar sheet with a thickness of 178 μm. Both ends of the channel space were cut in a triangular shape with lengths of 2.0 and 1.0 cm, respectively. The inlet frit was installed at the beginning end of the depletion wall and the length of the inlet frit was 3.0 cm from the sample inlet. A sheet membrane (model PLCGC) from Millipore Corp. (Billerica, MA, USA), regenerated cellulose with a molecular weight cutoff of 10 kDa, was layered above the accumulation wall.

Samples were injected with a Model 7125 loop injector from Rheodyne (Cotati, CA, USA) through the FI-AFlFFF channel inlet. Samples were delivered with a Model 305 HPLC pump from Gilson (Villers Le Bell, France) at 0.1 mL/min of sample flow rate, $\dot{V}_s$. Simultaneously, frit flow was delivered through the inlet frit by a Model M930 HPLC pump from Young-Lin Co. (Seoul, Korea). In the FI-AFlFFF channel, part of the flow (cross flow rate, $\dot{V}_c$) exits through the channel accumulation wall and is circulated to the frit flow ($\dot{V}_f$) with the connection of a fluid reservoir to minimize the pump pulse in between, as shown in Fig. 1. By decreasing the cross flow rate and frit flow rate simultaneously, the field strength applied to sample molecules can be gradually decreased according to the programming pattern used. Sample materials are eluted at the channel outlet (outflow rate, $\dot{V}_{out}$) and are monitored by a DAWN-DSP mulitangle light scattering detector and an Optilab DSP differential refractive index (DRI) detector from Wyatt Technology (Santa Barbara, CA, USA) in sequence as shown in Fig. 1. Filtered toluene was

used to calibrate the scattering intensity of the MALS instrument. The albumin (BSA) sample was used for the normalization of the MALS instrument and the measurement was made with by pumping albumin solution to the MALS instrument using a Model KDS 100 syringe pump from KD scientific (New Hope, PA, USA) at a flow rate of 0.10 mL/min. For the calculation of d*n*/d*c* of NaHA samples used in this study, RI signals were measured by directly injecting each NaHA solution through an Optilab DSP interferometric refractometer with the variation of its concentration and the calculation was made using DNDC5 software from Wyatt Technology. Calculated values of d*n*/d*c* for the two NaHA samples were 0.179 and 0.112 for samples A and B, respectively. For the calculation of molecular mass and the RMS radius, LS signals of the angles (4–10th) were processed with a third-order polynomial fitting using the Berry method of the Debye plot using ASTRA software from Wyatt Technology.

3. Results and discussion

Separation of the broad MW NaHA sample by the FI-AFlFFF channel has been carried out by a field programming technique in which the cross flow rate decreases during separation. Fig. 2 shows the superimposed plots representing three FI-AFlFFF fractograms, calculated molecular weight values from MALS detection, and RMS radius values at each time slice (or volume slice) obtained from NaHA sample A dissolved at three different temperatures (5 °C, 50 °C, and 90 °C). The three fractograms are represented with light scattering signals measured at 90 degrees. Since the cross flow during the programmed separation in FI-AFlFFF is circulated to the frit flow (as shown in Fig. 1), both flow rates (cross flow and frit flow) are the same, and therefore the channel outflow rate is always the same as the sample flow rate. The linear field decay pattern used for FI-AFlFFF separation is represented at the top of Fig. 2 and the detailed condition is as follows. The frit flow rate (=cross flow rate) begins at 2.0 mL/min for 3 min of an initial delay period in order to provide a sufficient hydrodynamic relaxation of the incoming sample components by applying a high field strength. After a short period of time (3 min), it linearly decreases to 0.5 mL/min over a period of 5 min, to 0.1 mL/min over 11 min, to 0.02 mL/min over 5 min, and it is then fixed at 0.02 mL/min until the end of elution. The optimization of this field decay pattern is based on the previous study [24]. The three samples treated at different temperature conditions appear to begin eluting after 10 min when the cross flow rate decreases to nearly 0.1 mL/min. As the dissolution temperature increases, NaHA molecules elute with a broader distribution and the peak maxima clearly shifts toward the longer elution time. If the degradation of NaHA molecules occurs significantly as the temperature increases, it will appear with an increase of scattering intensity at or around the beginning of elution (~20 min). This may not be visualized since light scattering intensity for larger MW components is stronger than that of smaller ones. However, the shift of the peak maxima to a longer retention time scale exhibits a possibility of structural variation or change in the molecular weight distribution of NaHA molecules by thermal stress unless aggregation of the molecules occurs. These will be explained by comparing MW or RMS radius values of the samples before and after treatment.

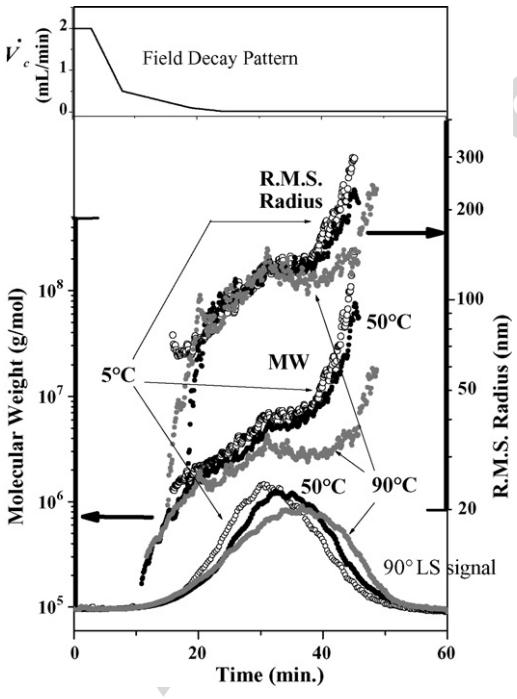

Fig. 2. Superimposed plots showing LS-90° signals of FI-AFlFFF/MALS, calculated molecular weights, and RMS radius of NaHA sample A treated at different dissolution temperature conditions (5 °C, 50 °C, and 90 °C). Symbols of open circles, filled circles with black color, and gray circles represent sample A treated at 5 °C, 50 °C, and 90 °C, respectively. On top of the figure, a linear decay pattern of field strength (cross flow rate) is plotted. Out flow rate is maintained at 0.1 mL/min throughout the runs. Details of the field decay pattern are explained in the text.

The molecular weight value of each time slice is calculated using the ASTRA software for the LS signals along with the concentration detector signals (DRI). The calculated MW values of the three sample A's are plotted above the fractograms in Fig. 2 and the MW scales are represented on the left axis. MW values for the sample dissolved at 5 °C (open circles) appear to increase smoothly as retention time increases. This represents the elution of NaHA molecules at an increasing order of MW during the run. (Hereafter, the samples are named with the following convention: sample A5 represents the sample A treated with the dissolution temperature 5 °C.) It is noted that MW values increase steadily until 40 min but then increase rapidly. This is due to the difference in the slopes of field decay during programming. However, the MW values appear to increase with the increase of retention time without a serious fluctuation, and this supports that size fractionation of sample A5 is carried out successfully with the programmed FI-AFlFFF throughout the run. While the MW distribution of sample A5 ranges from 10^6 g/mol to 10^8 g/mol, sample A50 (filled circles) shows a similar pattern but calculated MW values throughout the run are slightly smaller than those of sample A5. The calculated MW values at the beginning of the elution of sample A5 (until 16 min) are fluctuating so they are not included in Fig. 2. These fluctuations are often observed at both ends of the eluting peak in FlFFF–MALS experiments where concentrations of detected molecules are not high enough to collect sufficient LS signals at all angles. From

these observations, it is found that the current field programming condition of FI-AFlFFF can provide successful size fractionation of broad and ultrahigh MW NaHA molecules of the third order of magnitude (10^5–10^8 g/mol).

While MW distribution profiles of samples A5 and A50 are similar to each other, MW values of sample A90 are significantly different. Calculated MW values at each time slice become further reduced and large MW components (after 30 min) are retained longer than is expected. Moreover, the upper limit of MW for sample A90 appears to be reduced to $\sim 2 \times 10^7$ g/mol and MW values in the time slices 30–40 min do not increase, but slightly decrease. These observations may be explained as follows. The decrease of the calculated MW at time slices between 30 and 40 min can be thought of as a result from an elongated retention of extended NaHA species that is caused by high temperature dissolution. According to literature [5], the common forms of NaHA in the solid state are known to be a fully extended helix, a three-fold helix, and a compressed four-fold helix which are stabilized by hydrogen bonds between glycosidic linked monomers according to temperature and humidity. If the multiple helical structures can be loosened or dissociated, highly entangled NaHA species may undergo extension from a rather compact conformation or may disagglomerate into a less entangled structure. This change, if it occurs, results in the elongation of retention time, because polymers of a linear shape are retained in the flow FFF channel longer than those of a relatively compact or spherical shape. When RMS radius values of the three sample preparations are compared, they overlap until ~35 min as shown in the plot above the MW plots in Fig. 2. The reduction of the upper limit of MW for sample A90 may result from a possible chain disagglomeration. However, the reason for stagnation of the increasing trend of MW at the time interval of 30–40 min is not clear. It can be premised that eluting components during this time period (corresponding to $2–4 \times 10^6$ g/mol) contain a mixture of some unfolded and folded NaHA species of which the MW of the latter is larger. It could be expected that conformation of very high MW NaHA molecules ($> \sim 5 \times 10^6$ g/mol) is different from that of relatively smaller MW ones. However, with this result alone, it is not yet clear and will be explained later with more evidence on the MW dependence of RMS radius.

Fig. 3(a) is the superimposed plots of RMS radius versus MW for the three sample preparations. Apparently, NaHA molecules smaller than $\sim 4 \times 10^6$ g/mol (the dotted vertical line in Fig. 3(a) show larger RMS radius values when the dissolution temperature increases. This supports the premise that NaHA molecules at higher temperature conditions are extended to some degree. When RMS radius values are examined against MW, the slope of the plot represents conformational information of the molecules present in the solution. The overall slope calculated for each sample is shown in Fig. 3(a). The overall slope does not change much as the dissolution temperature increases from 5 °C to 50 °C. However, it significantly changes from 0.38 to 0.65 as the temperature increases from 50 °C to 90 °C. Based on the calculated slope values alone, it is likely that the molecular structure becomes more extended with temperature. Each regression line in Fig. 3(a) seems to represent only a certain MW interval but each slope value is calculated from all the data points that belong

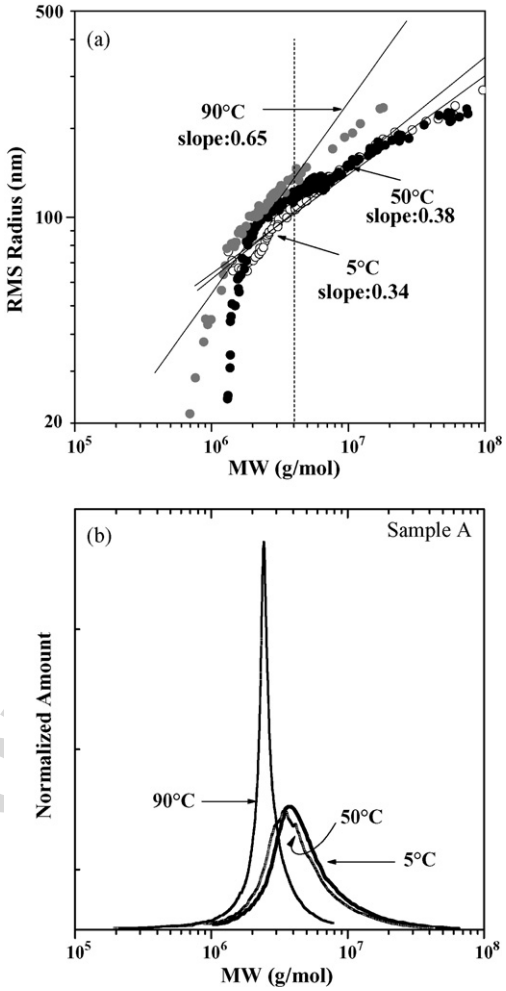

Fig. 3. (a) RMS radius vs. MW and (b) normalized MWD curves of sample A treated at the three different temperature conditions. Symbol representation follows the rule used in Fig. 2. Slope values in plot (a) are obtained from a linear regression over all data points of each temperature condition.

to each sample. Since the slope value depends on the interval selected, the structural determination can be different for different MW regimes. In the case of sample A50, the slope value (0.38) is calculated to be slightly larger than that of the sample A5 (0.34) while the apparent slope from the data points is smaller. The increase in the calculated slope value results from the regression over all the data points. However, most data points above $\sim 4 \times 10^6$ g/mol in sample A50 overlapped with those of sample A5. This shows that there is no large difference in molecular structure between the two samples (A5 and A50).

The slope of the data points in Fig. 3(a) can be divided into two regimes if examined closely. For instance, data points smaller than approximately 4×10^6 g/mol for samples A50 and A90 appear to have larger slopes but the others show smaller values. This represents that NaHA molecules may have at least two different structures depending on the range of molecular weight. The slope values for the two different MW regimes (smaller or larger than 4×10^6) are calculated individually. While the slope values for the smaller MW interval (1.5×10^6–4×10^6) are similar each other as 0.59, 0.57, and 0.55 for 5 °C, 50 °C, and 55 °C,

Table 1
Molecular weight and RMS radius values of the two NaHA samples with RSD ($n = 3$) at different dissolving temperatures from FI-AFlFFF/MALS/DRI

Temperature	5 °C	50 °C	90 °C
(a) Sample A			
Mw (g/mol)	$(6.23 \pm 0.22) \times 10^6$	$(5.05 \pm 0.09) \times 10^6$	$(2.67 \pm 0.10) \times 10^6$
Mn (g/mol)	$(4.35 \pm 0.27) \times 10^6$	$(3.29 \pm 0.18) \times 10^6$	$(2.25 \pm 0.13) \times 10^6$
Mw/Mn	1.45 ± 0.11	1.60 ± 0.09	1.26 ± 0.07
RMS radius (nm)	156.1 ± 11.9	142.7 ± 7.3	130.0 ± 8.2
Temperature	5 °C	50 °C	90 °C
(b) Sample B			
Mw (g/mol)	$(8.01 \pm 0.49) \times 10^6$	$(6.78 \pm 0.18) \times 10^6$	$(3.58 \pm 0.03) \times 10^6$
Mn (g/mol)	$(4.82 \pm 0.37) \times 10^6$	$(4.55 \pm 0.15) \times 10^6$	$(3.08 \pm 0.13) \times 10^6$
Mw/Mn	1.89 ± 0.16	1.50 ± 0.05	1.14 ± 0.05
RMS radius (nm)	193.6 ± 14.0	160.7 ± 8.8	112.9 ± 4.2

respectively, those for the MW regime larger than 4×10^6 are 0.27, 0.24, and 0.39 in the order of increasing temperature. The molecules are likely to have a rather linear structure for NaHA MW smaller than $\sim 4 \times 10^6$, but an entangled or rather compact structure for the larger MWs. In the case of sample A90, most NaHA molecules appear to be smaller than this limiting MW and thus become linear in solution under high temperature. If an isolation of these molecules below a certain MW regime can be properly achieved by some means, it will be helpful to elucidate the difference in molecular structure. This is not in the scope of the current study and will be attempted soon. The molecular weight distributions of the thermally treated samples are compared in Fig. 3(b). This shows that the MWD of the NaHA sample A is significantly transformed into a narrow distribution with the reduction of average MW to 2.67 (±0.10) $\times 10^6$ g/mol (90 °C) from 6.23 (±0.22) $\times 10^6$ (5 °C). The calculated MW values are listed in Table 1 along with polydispersity (Mw/Mn) and RMS radii. Three measurements were taken for all experiments.

The same experiments were carried out with sample B produced by a different batch (purification) from the manufacturer. In Fig. 4, the three LS-90° signals of FI-AFlFFF fractograms, calculated MW, and RMS radius values are plotted. In the case of sample B, the three fractograms from samples B5, B50, and B90 show similar retention profiles. While the NaHA sample B5 which was dissolved at 5 °C appears to have a similar MW distribution compared to that of sample A5, the MW value of the peak maxima for the treated sample B5 in Fig. 4 is approximately $\sim 1 \times 10^7$ g/mol which is larger than that of sample A5 ($6–7 \times 10^6$) in Fig. 2. However, the rate of MW increase within 20–40 min for sample B90 is somewhat slow, and the calculated MW and RMS radius values of higher MW components of the sample B are significantly reduced when the dissolution temperature increases. This shows that high MW components ($>10^7$ g/mol) of sample B are more influenced by the thermal stress. The plots in Fig. 5(a) show the rate of increase of RMS radius with respect to the increase of MW represent that the slope increases from 0.42 (open circles) to 0.60 (grey circles) when the dissolution temperature increases from 5 °C to 90 °C, respectively. When we look closely at the MW distribution of sample B90 in Fig. 4, it is found that the majority of NaHA molecules eluted by the FI-AFlFFF run corresponds to the MW range between $\sim 2 \times 10^6$ and $\sim 6 \times 10^6$ g/mol. Though the data points (grey circles) of sample B90 shown in Fig. 5(a) appear to be scattered throughout the entire MW range, they are mostly distributed within the short MW interval and this results in the calculation of the slope as 0.60. This result supports that the conformation of NaHA molecules becomes extended with the increase of dissolution temperature as observed for sample A. The differential MW distribution curves of sample B at different temperature conditions are plotted in Fig. 5(b) and the results are similar to that observed for sample A. Calculated molecular weights along with RMS radius values are listed in Table 1.

In Fig. 6, the effect of membrane filtration on the MW distribution is examined with FI-AFlFFF/MALS. Sample A5 is filtered by membranes with pore sizes of 0.45 μm and 0.2 μm separately. Fig. 6(a) shows the superimposed LS-90° signals obtained from sample A5 with or without membrane filtration at the same flow rate condition used in Fig. 2. The LS signal intensities are significantly reduced when sample A5 is filtered

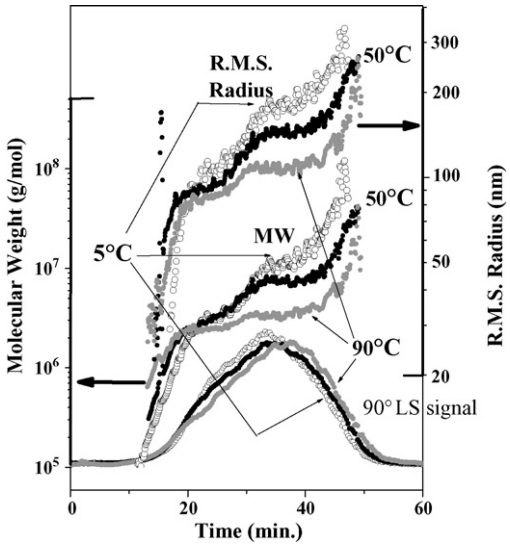

Fig. 4. Superimposed plots showing LS-90° signals of FI-AFlFFF/MALS, calculated molecular weights, and RMS radius of NaHA sample B treated at different dissolution temperature conditions (5 °C, 50 °C, and 90 °C). Symbol representation follows the rule used in Fig. 2.

Table 2
Effect of filtration on molecular weight and RMS radius values of the NaHA sample A with RSD ($n = 3$)

Temperature	Without filtration	Filtration at 0.45 μm	Filtration at 0.2 μm
Mw (g/mol)	$(6.23 \pm 0.22) \times 10^6$	$(3.55 \pm 0.20) \times 10^6$	$(3.10 \pm 0.192) \times 10^6$
Mn (g/mol)	$(4.35 \pm 0.27) \times 10^6$	$(2.57 \pm 0.13) \times 10^6$	$(2.31 \pm 0.13) \times 10^6$
Mw/Mn	1.45 ± 0.11	1.39 ± 0.06	1.24 ± 0.05
RMS radius (nm)	156.1 ± 11.9	144.6 ± 7.7	141.7 ± 4.2

by a membrane with a 0.45 μm pore size, and those of the sample treated with 0.2 μm are further reduced. While the LS signal intensities are significantly reduced with the filtration process, the MW values calculated for each sample preparation in Fig. 6(a) show good overlap among the three samples and this

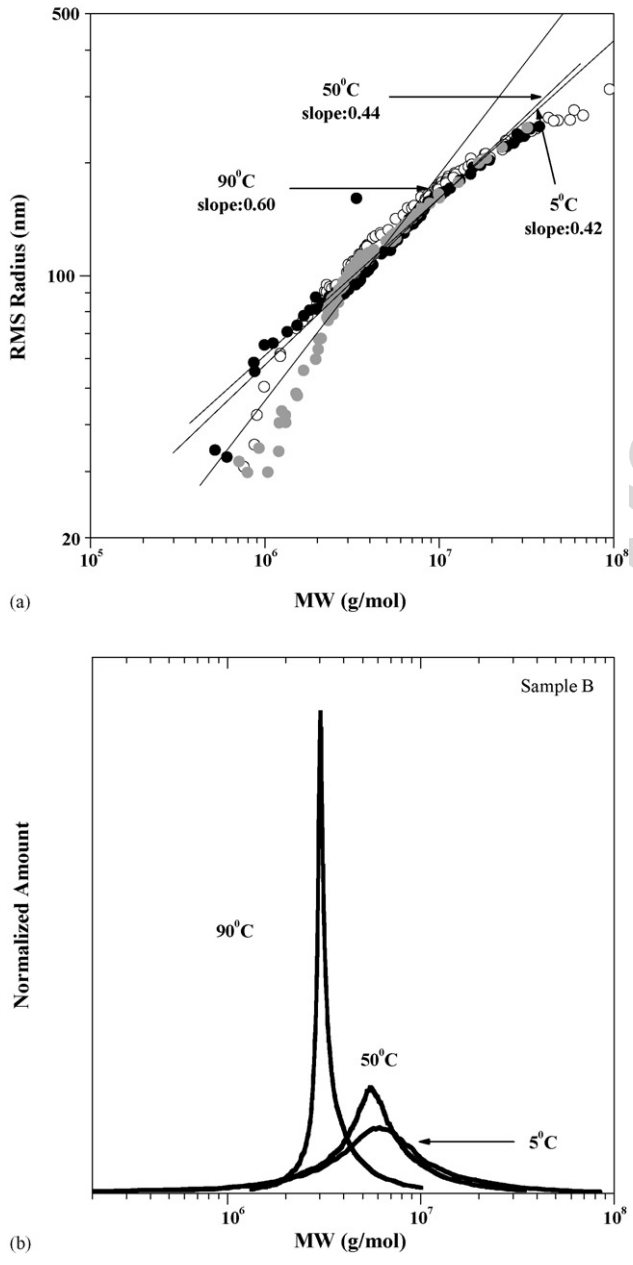

Fig. 5. (a) RMS radius vs. MW and (b) normalized MWD curves of sample B treated at the three different temperature conditions.

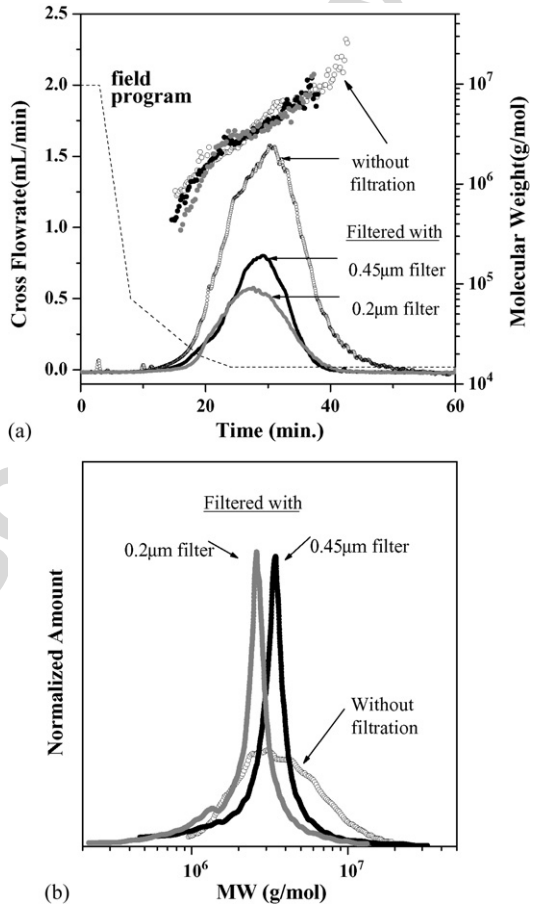

Fig. 6. Effect of sample filtration on MWD of sample A dissolved at 5 °C. Filtration is achieved by membrane filters with pore sizes of 0.2 μm and 0.45 μm. (a) Comparison of FI-AFlFFF fractograms (plotted with LS-90° signals) and calculated MW values along with field decay patterns. The run condition is the same used in Fig. 3. (b) Normalized MWD of sample A before and after filtration.

may represent a low possibility of structural deformation during the filtration process. However, there is a large difference in MWDs with filtration as shown in Fig. 6(b). It is found that a large amount is lost during filtration and the MWD becomes narrow with a change in average molecular weight. Table 2 compares the average MW values of sample A5 before and after filtration. It shows a clear decrease in the weight average and number average values of MW when filtration with 0.45 μm is applied. In addition, polydispersity values decrease from 1.45 ± 0.11 to 1.39 ± 0.06 and 1.24 ± 0.15. Sample filtration is commonly utilized in SEC analysis, and FlFFF provides the advantage of analyzing ultrahigh molecular weight polymers without losing information caused by the filtration process.

4. Conclusion

In this study, FI-AFlFFF/MALS/DRI has been utilized for the separation and size characterization of broad and ultrahigh molecular weight (10^5–10^8 in Da) NaHA samples and for the study of variation in the molecular conformation of NaHA in aqueous solutions by dissolving NaHA at different temperatures. The process demonstrates that high molecular weight NaHA components ($>\sim10^7$ Da) appear to transform into an extended structure from a compact or multiple helical structure when they are dissolved at an elevated temperature (90 °C). Also studied was the influence of membrane filtration of NaHA samples on MWD, which shows a significant loss of NaHA molecules along with the change of MWD. This demonstrates that Thus, any artifact encountered when obtaining an accurate MWD due to a filtration process can be completely removed with the use of a separation channel without having packing materials in the FlFFF system. This study shows the great potential of FI-AFlFFF, which is advantageous in handling ultrahigh molecular weight components without stopping the migration flow and in characterizing MWD and structural information on broad and ultrahigh molecular weight polymers.

Acknowledgements

This study was supported by the Korea Research Foundation Grant (KRF-2004-015-C00348) and, also, partly by a grant from the Korea Science and Engineering Foundation through the Center for Bioactive Molecular Hybrids (CBMH) at Yonsei University.

References

[1] B. Yeung, D. Marecak, J. Chromatogr. A. 852 (1999) 573.
[2] Z. Iqbal, J.M. Midgley, D.G. Watson, S.D. Karditsas, G.N. Dutton, W. Wilson, Pharm. World Sci. 19 (1997) 246.
[3] K.P. Vercruysse, G.D. Prestwich, Crit. Rev. Ther. Drug Carrier Syst. 15 (1998) 513.
[4] E.D.T. Atkins, C.F. Phelps, J.K. Sheehan, Biochem. J. 128 (1972) 1255.
[5] P. Livant, L. Roden, R. Krishna, Carbohydr. Res. 237 (1992) 271.
[6] N. Motohash, Y. Nakamichi, I. Mori, H. Nishijawa, J. Umemoto, J. Chromatogr. 435 (1988) 335.
[7] H. Sasari, T.Y. Konttinen, S. Santavirta, Med. Sci. Res. 18 (1989) 99.
[8] R. Takahashi, S. Al-Assaf, P.A. Williams, K. Kubota, A. Okamoto, K. Nishinari, Biomacromolecules 4 (2003) 404.
[9] G. Karlson, R. Bergman, J. Chromatogr. A. 986 (2003) 67.
[10] N. Motohashi, Y. Nakamichi, I. Mori, H. Nishikawa, K. Umemoto, J. Chromatogr. 435 (1988) 335.
[11] S. Hayase, Y. Oda, S. Honda, K. Kakehi, J. Chromatogr. A. 768 (1997) 295.
[12] J.C. Giddings, Anal. Chem. 53 (1981) 1170A.
[13] J.C. Giddings, Science 260 (1993) 1456.
[14] M.E. Schimpf, K.D. Caldwell, J.C. Giddings, Field-Flow Fractionation Handbook, Wiley Interscience, N.Y, 2000.
[15] K.-G. Wahlund, J.C. Giddings, Anal. Chem. 59 (1987) 1332.
[16] S.K. Ratanathanawongs, J.C. Giddings, Anal. Chem. 64 (1992) 6.
[17] H. Thielking, D. Roessner, W.-M. Kulicke, Anal. Chem. 67 (1995) 3229.
[18] B. Wittgren, K.-G. Wahlund, J. Chromatogr. A. 760 (1997) 205.
[19] B. Hecker, P.D. Fawell, A. Jefferson, J.B. Farrow, J. Chromatogr. A. 837 (1999) 139.
[20] L. Picton, I. Bataille, G. Muller, Carbohydr. Polym. 42 (2000) 23.
[21] C. Duval, D.L. Cerf, L. Picton, G. Muller, J. Chromatogr. B. 753 (2001) 115.
[22] W. Fraunhofer, G. Winter, C. Coester, Anal. Chem. 76 (2004) 1909.
[23] M. Andersson, B. Wittgren, H. Schagerlof, D. Momcilovic, K.-G. Wahlund, Biomacromolecules 5 (2004) 97.
[24] H. Lee, H. Kim, M.H. Moon, J. Chromatography A 1089 (2005) 203.
[25] M.H. Moon, H.S. Kwon, I. Park, Anal. Chem. 69 (1997) 1436.
[26] M.H. Moon, P.S. Williams, H. Kwon, Anal. Chem. 71 (1999) 2657.
[27] M.H. Moon, D. Kang, I. Hwang, P.S. Williams, J. Chromatogr. A. 955 (2002) 263.
[28] D.J. Kang, M.H. Moon, Anal. Chem. 76 (2004) 3851.